


Enhancing entanglement with the generalized elephant quantum walk from localized and delocalized states

Caio B. Naves^{1,*}, Marcelo A. Pires^{2,†}, Diogo O. Soares-Pinto^{1,‡} and Sílvia M. Duarte Queirós^{3,§}

¹*Instituto de Física de São Carlos, Universidade de São Paulo, CP 369, 13560-970 São Carlos, São Paulo, Brazil*

²*Departamento de Física, Universidade Federal do Ceará, 60451-970 Fortaleza, Brazil*

³*National Institute of Science and Technology for Complex Systems, 22290-180 Rio de Janeiro, Brazil*

 (Received 31 March 2022; revised 29 June 2022; accepted 7 September 2022; published 6 October 2022)

Recently, a generalization of a nonstandard step operator named the elephant quantum walk (EQW) was introduced. With proper statistical distribution for the steps, that generalized EQW (gEQW) can be tuned to exhibit a myriad of dynamical scaling behavior ranging from standard diffusion to hyperballistic spreading. In this work, we study the influence of the statistics of the step size and the delocalization of the initial states on the entanglement entropy of the coin. Our results show that the gEQW generates maximally entangled states for almost all initial coin states and coin operators considering initially localized walkers, and for the delocalized ones, taking the proper limit, the same condition is guaranteed. Differently from all the previous protocols that produce highly entangled states via QWs, this model is not upper bounded by ballistic spreading and hence opens prospects for applications of dynamically disordered QWs as a robust maximal entanglement generator in programmable setups that ranges from slower than ballistic to faster than ballistic.

DOI: [10.1103/PhysRevA.106.042408](https://doi.org/10.1103/PhysRevA.106.042408)

I. INTRODUCTION

By making use of the quantum principle of superposition, the space-time evolution of a quantum particle—a walker—on a grid is understood to be exponentially more powerful than its inspiring classical random walk analog [1–3] in scientific and technological applications such as search algorithms and transport phenomena, namely, photosynthetic energy [4–6] and coherent transport [7–12], among many other implementations that are either experimental [13–16] or closely related to applications of quantum computation [17].

Since the introduction of the first quantum walk (QW) [1], a myriad of variants and extensions has been introduced (see references above); primarily, they aimed to study diffusion-scale properties and search performance enhancement regarding the optimal Grover’s algorithm [18]. Being a quantum system described by the composition of two subspaces, i.e., walker and coin, the QW problem is naturally suitable to the analysis of a pure quantum feature: entanglement. Nonetheless, the measurement between its subspaces only took place some years afterwards [19]. On the other hand, quantum features do not boil down to entanglement, e.g., the localization conditions are another crucial property for the understanding of quantum effects [20].

In the present manuscript, we analyze the outcome on the entanglement entropy for a general disordered quantum walk

model that is able to describe a wide range of dynamical features—from normal (such as a classical random walker) to hyperballistic diffusion, as experimentally verified in hybrid ordered-disordered photonic lattices [21]—considering different localization status.

The remainder of this text is organized as follows: in Sec. II, we provide a concise review of the aforementioned subject matters, which are at the core of the present study; in Sec. III, we introduce the model and, in Sec. IV, we report our results and discuss them. At last, in Sec. V, we provide some concluding words in our study and point out further avenues of research.

II. LITERATURE REVIEW

The canonical discrete-time quantum walk was pioneered in 1993 [1]. It is a lattice-based model exhibiting interesting features [5–10] when compared with the classical random walk (CRW). First, in its standard version, the QW is quadratically faster than the CRW; second, it shows a non-Gaussian bimodal distribution while the CRW displays the usual Gaussian distribution. Apart from this, the QW is able to entangle their internal (spin) and external (position) degrees of freedom. This feature can be quantified by the entanglement entropy S_E whose value was first numerically estimated to be 0.872 in the asymptotic regime [19]. Such a value was posteriorly demonstrated mathematically [22] and experimentally [23–25].

The nonstandard versions of the QW are even more interesting. For instance, in 2012 [26], it was numerically shown that QWs with random temporal disorder can be used as a maximal entanglement generator. This

*caio.naves@usp.br

†piresma@cbpf.br

‡dosp@ifsc.usp.br

§sdqueiro@cbpf.br; on leave of absence from CBPF, Brazil.

counterintuitive result was demonstrated mathematically in 2013 [27] and experimentally in 2018 [23]. Further works have provided an analysis of the entanglement considering several protocols of disorder embedded either in the coin operator [28–42] or in the step operator [43–45]. With some exceptions, the overwhelming majority of these works focused on QW dynamics from local initial states. In Ref. [46], it was shown that for disorder-free QWs, delocalization increases the number of initial states which reach maximal asymptotic entanglement.

At this point, a question arises: How does the entanglement in QWs change in the presence of both disorder and delocalization? This issue was briefly and partially addressed when temporal disorder was embedded in the coin operator [30], where it was shown that the maximal asymptotic entanglement is still achieved. However, the aforementioned question is still open when temporal disorder is introduced in the step operator.

Even though QWs with temporal disorder in the coin operator have been studied for a much longer time [5–10], the QWs with temporal disorder in the displacement operator exhibit an interesting phenomenology [43–45,47–57]. In some circumstances, both types of models share some similarities, for instance, the achievement of maximal asymptotic entanglement from local states [26,27,43,44]. However, up to now, only QWs with dynamic disorder in the displacement operator have been able to produce hyperballistic dynamics [52]. For QWs with random disorder in the coin operator, the boosting of entanglement takes place with an upper-bounded ballistic spreading [26,27,42]. Such impasse can be avoided when the temporal disorder is present in the shift operator. Specifically, recently [43] a protocol—the generalized elephant quantum walk (gEQW)—was presented that is able to exhibit both amplification of entanglement and tunable spreading from slower than ballistic to faster than ballistic. However, the authors have only considered some specific and local initial states. In order to move towards potential future applications, it is necessary to answer the following: Is the enhancement of the entanglement in the gEQW robust or only valid under the specific conditions? As will be shown, in this work we provide a firmer conclusion: The asymptotic strengthening of the entanglement between the degrees of freedom in a quantum walk is robustly achieved for the protocol of the gEQW dynamics with general coin operators and from both local and delocalized initial states.

III. MODEL

A. The standard coined discrete-time quantum walk

The Hilbert space of the one-dimensional coined discrete-time quantum walk (DTQW) is composed of the position space of the walker, $\mathcal{H}_p = \text{span}(\{|x\rangle, x \in \mathbb{Z}\})$, and the quantum coin space, $\mathcal{H}_c = \text{span}(|\uparrow\rangle, |\downarrow\rangle)$, so that the total Hilbert space of the walker is $\mathcal{H} = \mathcal{H}_p \otimes \mathcal{H}_c$ [8,58,59]. Consequently, the state of the walker reads

$$|\psi(t)\rangle = \sum_{x=-\infty}^{\infty} |x\rangle (c_{\uparrow}(x,t)|\uparrow\rangle + c_{\downarrow}(x,t)|\downarrow\rangle), \quad (1)$$

whose density operator is

$$\rho(t) = \sum_{x,x'} |x\rangle\langle x'| \otimes \begin{pmatrix} c_{\uparrow}(x,t)c_{\uparrow}^*(x',t) & c_{\uparrow}(x,t)c_{\downarrow}^*(x',t) \\ c_{\downarrow}(x,t)c_{\uparrow}^*(x',t) & c_{\downarrow}(x,t)c_{\downarrow}^*(x',t) \end{pmatrix}, \quad (2)$$

where $c_{\uparrow,\downarrow}^*$ denotes the complex conjugate of $c_{\uparrow,\downarrow}$.

The unitary evolution of a coined DTQW involves the action of two operators. Explicitly, we have one operator for the quantum coin, the *coin toss operator*, and the *shift operator*, respectively. The purpose of the coin toss operation is to put the coin state in a superposition of its possible states—a quantum analogy of the coin tossing in a classical random walk. In the one-dimensional DTQW, the coin toss operator is a two-by-two unitary matrix, given in its most general form by

$$C_2 = \begin{pmatrix} \cos \theta & \sin \theta e^{i\beta} \\ \sin \theta e^{i\gamma} & -\cos \theta e^{i(\gamma+\beta)} \end{pmatrix}, \quad (3)$$

with $\theta = \pi/4$, $\beta = \gamma = 0$ yielding the Hadamard operator, i.e.,

$$C_2 = H = \frac{1}{\sqrt{2}} \begin{pmatrix} 1 & 1 \\ 1 & -1 \end{pmatrix}. \quad (4)$$

In this work, we also employ the *Kempe coin* [8], a class of non-Hermitian coin toss operators where $\beta = \gamma = \pi/2$,

$$C_2 = C_k(\theta) = \begin{pmatrix} \cos \theta & i \sin \theta \\ i \sin \theta & \cos \theta \end{pmatrix}. \quad (5)$$

Regarding the shift operator, it updates the position state of the walker accordingly with its coin state. On the one-dimensional lattice,

$$S = \sum_{x=-\infty}^{\infty} |x+1\rangle\langle x| \otimes |\uparrow\rangle\langle\uparrow| + |x-1\rangle\langle x| \otimes |\downarrow\rangle\langle\downarrow|. \quad (6)$$

Notice that the shift operator associates the up (down) state with a displacement to the right (left).

The discrete-time quantum walk one-step unitary operator is

$$U = S(\mathbb{I}_p \otimes C), \quad (7)$$

where \mathbb{I}_p is the identity operator in the position space. A recursive equation for the coefficients of the state of the walker is found if we apply the unitary operator given by Eq. (7) on Eq. (1), leading to

$$\begin{aligned} c_{\uparrow}(x,t) &= \cos \theta c_{\uparrow}^{x-1}(t-1) + \sin \theta e^{i\beta} c_{\downarrow}^{x-1}(t-1), \\ c_{\downarrow}(x,t) &= \sin \theta e^{i\gamma} c_{\uparrow}^{x+1}(t-1) - \cos \theta e^{i(\beta+\gamma)} c_{\downarrow}^{x+1}(t-1), \end{aligned} \quad (8)$$

where we have shortened $c_{\uparrow,\downarrow}(x \pm 1, t-1)$ to $c_{\uparrow,\downarrow}^{x \pm 1}(t-1)$. Recursive relations (8) are important tools for the analytical derivation of the asymptotic properties of the quantum walk and are quite useful to perform numerical simulations as well, as occurs in the Schrödinger approach method [7].

One important point one must be aware of is that in comparison with the classical random walk, the asymptotic properties are both initial coin-state and coin-operator dependent. In other words, the outcome of a given implementation depends on the initial setting. Nonetheless, one of the remarkable facts about quantum walks is that the asymptotic behavior

of the standard deviation of the position grows linearly, i.e., ballistically, with time, $\sigma \approx t$, whereas in the random walk, it goes as $\sigma \approx t^{1/2}$ [58,59]. That represents a quadratic gain in the diffusion rate over the classical random walk and it is solely due to the fact that a quantum walk makes use of the superposition principle. Another fact is that we can generate entanglement between the coin and the position degrees of freedom, a genuinely quantum feature of quantum walks, which in some cases can get to its maximal value.

B. The generalized elephant quantum walk

The quantum walk model that we consider consists of a noisy unitary evolution of a DTQW on a lattice where the step sizes are randomly chosen, i.e., a model devised in Ref. [43], called the generalized elephant quantum walk (gEQW). This model is an extension of the elephant quantum walk [52], i.e., a quantum walk inspired by the classical non-Markovian elephant random walk where the walker remembers its previous steps, giving a variety of diffusion characteristics [60]. Here, the one-dimensional (1D) shift operator reads

$$S_t = \sum_{x=-\infty}^{\infty} |x + \Delta_t\rangle\langle x| \otimes |\uparrow\rangle\langle\uparrow| + |x - \Delta_t\rangle\langle x| \otimes |\downarrow\rangle\langle\downarrow|, \tag{9}$$

where S_t is the shift operator at time step t and Δ_t is the step size chosen in the same time instant. In this way, for every time instant, we will have a random unitary operator given by Eq. (7), with S_t in place of S , using the coin operators as Eq. (4) and Eq. (5) in the same manner.

We can interpret a random unitary evolution as a noisy open evolution where one observes, at each time step, which unitary operator was selected by the environment. Let \mathcal{H}_E be the Hilbert space of the environment and $\{|\Delta_j\rangle, j = 1, \dots, t\}$ be a spanning set of it. Given that the system-environment state $\rho_{S,E} \in \mathcal{H}_S \otimes \mathcal{H}_E$ is closed, it evolves through a unitary operator U ,

$$U = \sum_{j=1, \dots, t} U_j \otimes |\Delta_j\rangle\langle\Delta_j|. \tag{10}$$

Supposing that the environment state is given by $|\psi_E(t)\rangle = \sum_{j=1, \dots, t} \sqrt{p(\Delta_j)} |\Delta_j\rangle$, then the total state evolves as

$$\rho_{S,E}(t+1) = \sum_{j,j'} \sqrt{p(\Delta_j)} \sqrt{p(\Delta_{j'})} U_j \rho_S(t) U_{j'}^\dagger \otimes |\Delta_j\rangle\langle\Delta_{j'}|. \tag{11}$$

Performing a projective measurement $P_t = |\Delta_t\rangle\langle\Delta_t|$ and a partial trace over the environment degree of freedom, we obtain the following unnormalized system state:

$$\rho_S(t+1) = p(\Delta_t) U_t \rho_S(t) U_t^\dagger, \tag{12}$$

whose norm $p(\Delta_t)$ is the probability that the state $U_t \rho_S(t) U_t^\dagger$ was selected from the statistical mixture $\sum_j p(\Delta_j) U_j \rho_S(t) U_j^\dagger$.

The probability distribution used for choosing the steps sizes is a discretized version of the q -exponential distribution [61] (see Fig. 1),

$$\text{Pr}(\Delta_t) = e_q(\Delta_t) \equiv \tau_t [1 - (1 - q)\Delta_t]^{1/1-q}, \tag{13}$$

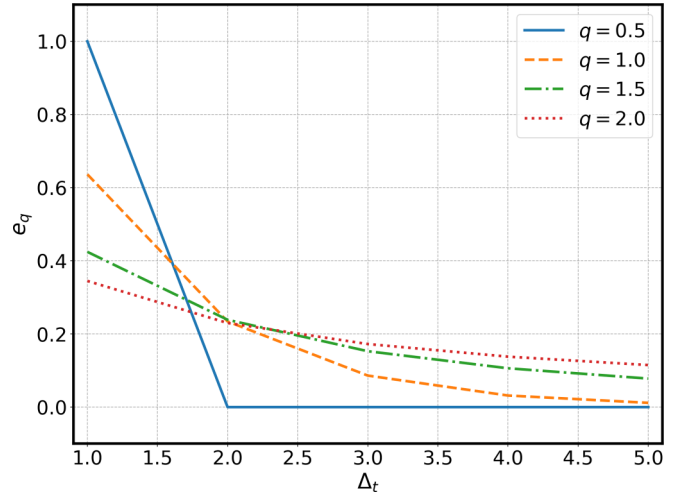


FIG. 1. The q -exponential probability distribution for some values of q .

with $\Delta_t \in [1, 2, \dots, t]$, τ_t a time-dependent normalization factor, and support given by

$$\text{supp}[e_q(x)] = \begin{cases} [0, \frac{1}{1-q}], & q \leq 1 \\ [0, \infty], & q > 1. \end{cases} \tag{14}$$

It is worth noting some limiting cases of the q -exponential probability distribution. For instance, when we set $q = 1/2$, it reads

$$e_{1/2}(\Delta_t) = \tau_t \left(1 - \frac{\Delta_t}{2}\right)^2. \tag{15}$$

Looking at Eq. (14), we see that $\Delta_t \leq 2$, where $e_{1/2}(\Delta_t = 1) = 1$ and $e_{1/2}(\Delta_t = 2) = 0$. Therefore, with $q = 1/2$, only unit step sizes are possible, matching with the standard DTQW. On the other hand, when $q = 1$, we get a decreasing exponential in the step sizes,

$$\lim_{q \rightarrow 1} e_q(\Delta_t) = \tau_t e^{-\Delta_t}. \tag{16}$$

Lastly, taking the limit of q going to infinity, we get the uniform distribution,

$$\lim_{q \rightarrow \infty} e_q(\Delta_t) = \frac{\tau_t}{t}, \tag{17}$$

characterizing the elephant quantum walk (EQW). Looking through the open evolution perspective, the q -exponential distribution gives us a versatile way to model a myriad of quantum walks ranging from the deterministic evolution, corresponding to the standard DTQW, to the completely random one, namely, the EQW.

In order to compare the degree of dispersion of a quantum walker, the asymptotic limit of the variance of the position was analyzed [43]. It is expected that its limiting behavior obeys

$$\text{Var}_X(t) = \sigma_X^2 \approx t^\alpha, \quad t \gg 1, \tag{18}$$

where α is called the *diffusion exponent*. By taking the logarithm of the position variance graph, it is possible to estimate the diffusion exponent and compare the quantum walks dispersion for different values of q . We must recall that the

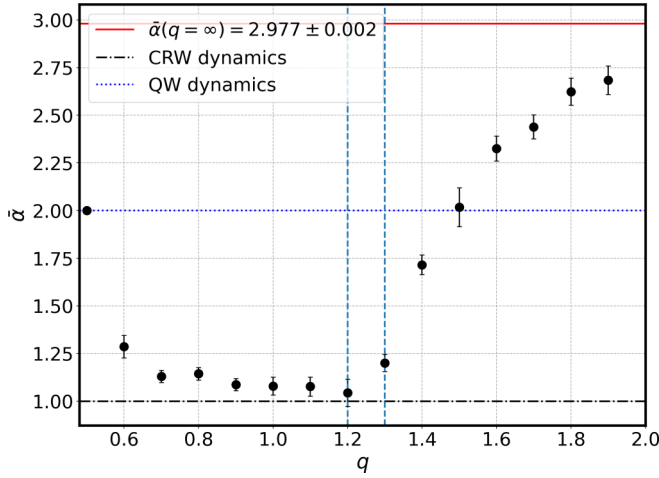


FIG. 2. Mean diffusion exponent as a function of the q parameter considering the quasistationary part of the evolution using the Kempe coin given by Eq. (5) with $\theta = \pi/4$ and the initial quantum walker state $|\psi(0)\rangle = |0\rangle \otimes (|\uparrow\rangle + |\downarrow\rangle)/\sqrt{2}$. The dashed line and dash-dotted line indicate the standard DTQW diffusion exponent $\alpha = 2$ and the classical random walk diffusion $\alpha = 1$, respectively. The vertical lines indicate the range of q above which the QW has an increasingly faster spreading. The red line gives us the value of the EQW's diffusion exponent $\bar{\alpha} = 2.977 \pm 0.002$.

evolution of this type of DTQW is random, in the sense that for a given time instant, the unitary operator can be different for different runs of the quantum walk. Consequently, the most appropriate is to consider the average diffusion exponent.

In Fig. 2, we have the mean diffusion exponent as a function of q , $\bar{\alpha}(q)$, in the range $[0.5, 1.9]$, considering only the quasistationary part of the quantum walks evolution. We also considered the value of the mean diffusion exponent for $q = \infty$. The behavior of the curve defined by the data points is similar to that obtained in Ref. [43]. For $q > 1.3$, the diffusion exponent starts increasing and it reaches its asymptotic hyperballistic limit, $\bar{\alpha} = 3$. Bear in mind that $q = \infty$ corresponds to the uniform distribution case, i.e., strong randomness in the step sizes leads the quantum walk to a hyperballistic regime, whereas weak randomness can lead it either to the standard DTQW ballistic regime or to the random walk diffusion.

In Ref. [43], it was shown that considering some values of q different from $q = 1/2$ and employing the von Neumann entropy as a purity quantifier of the coin state, the gEQW produces maximally entangled coin states when using the Kempe coin operator given by Eq. (5) with $\theta = \pi/4$ (see Fig. 5 in Ref. [43]). The questions we address are as follows: What if that result depends on the initial state of the coin? Is it coin-operator dependent as well? How does the average entropy change when we change the q -exponential distribution, i.e., the amount of disorder?

In the next section, we analyze the entanglement between the coin and position degrees as a function of the coin initial state and coin-operator parameters in the gEQW, taking initially localized and Gaussian delocalized walker states. After that, we investigate how the generalized elephant quantum walk goes to the quasistationary regime.

IV. RESULTS AND DISCUSSION

A. Coin entanglement entropy in the gEQW

The von Neumann entropy of a quantum state is defined as [62]

$$S_E \equiv -\text{tr}(\rho \log_2 \rho) = -\sum_i \lambda_i \log_2 \lambda_i, \quad (19)$$

with λ_i being the eigenvalues of the density matrix, ρ . We choose to consider the von Neumann entropy of the coin density matrix because it is a two-level system and the simplest part of the position-coin bipartition.

The coin density matrix is given by

$$\rho_c(t) \equiv \text{tr}_x[\rho(t)] = \begin{pmatrix} A(t) & B(t) \\ B^*(t) & C(t) \end{pmatrix}, \quad (20)$$

where $A(t) = \sum_x |c_\uparrow(x, t)|^2$, $B(t) = \sum_x c_\uparrow(x, t)c_\downarrow^*(x, t)$, and $C(t) = \sum_x |c_\downarrow(x, t)|^2$. In order to find the coin-state coefficients in the gEQW, we have to change the recursive relations of Eq. (8) to

$$c_\uparrow^x(t) = \cos \theta c_\uparrow^{x-\Delta t}(t-1) + \sin \theta e^{i\beta} c_\downarrow^{x-\Delta t}(t-1), \quad (21)$$

$$c_\downarrow^x(t) = \sin \theta e^{i\gamma} c_\uparrow^{x+\Delta t}(t-1) - \cos \theta e^{i(\beta+\gamma)} c_\downarrow^{x+\Delta t}(t-1). \quad (22)$$

Accordingly, the von Neumann entropy of the coin is given by

$$S_E = -\lambda_+ \log_2 \lambda_+ - \lambda_- \log_2 \lambda_-, \quad \text{with} \quad (23)$$

$$\lambda_\pm = \frac{1}{2}(1 \pm \sqrt{1 - 4(AC - |B|^2)}), \quad (24)$$

where we used the fact that $\text{tr}[\rho_c(t)] = 1 \rightarrow A(t) + C(t) = 1, \forall t$.

As a way to study the entanglement generation as a function of the initial parameters, throughout this work we have considered the time-averaged entanglement entropy taking only the quasistationary part of the entanglement evolution. It is expected that after an initial increase, the entanglement entropy reaches, at least, an average constant value [27,30]. The quasistationary regime depends on the type of quantum walk, initial state and coin operator. Therefore, the time-averaged entanglement entropy was determined individually for each evolution analyzed here by looking at the whole entanglement entropy evolution.

First, we study the time-averaged entanglement entropy as a function of the θ parameter in the Kempe coin operator, given by Eq. (5), and the polar angle Ω on the Bloch sphere of the coin initial state,

$$|\psi_c(0)\rangle = \cos\left(\frac{\Omega}{2}\right)|\uparrow\rangle + e^{i\phi/2} \sin\left(\frac{\Omega}{2}\right)|\downarrow\rangle, \quad (25)$$

with $q \rightarrow \infty$, the elephant quantum walk scenario, and ϕ set to zero. From Fig. 3(a), we see that the blue plateau indicates that the average entanglement entropy reaches its maximum value for almost all initial states and Kempe coin operators, which is something that does not happen when we have the standard discrete-time quantum walk [see, e.g., Fig. 3(b)]. Using a different value of q , e.g., $q = 1$, a similar result is obtained; see Fig. 3(c). These results, together with that

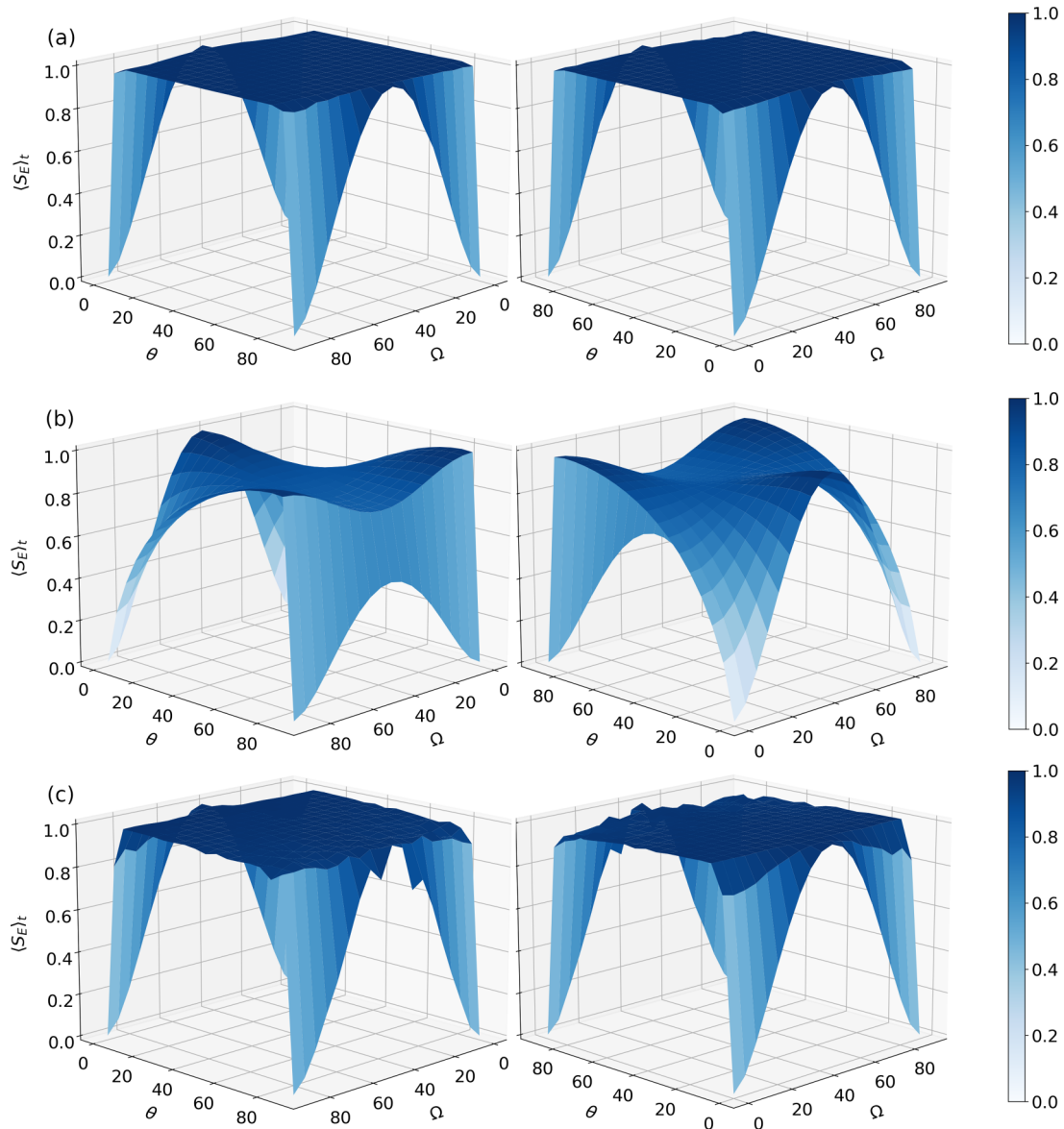


FIG. 3. Time-averaged entanglement entropy as a function of the θ (deg) parameter in the Kempe coin operator given by Eq. (5) and the Bloch polar angle Ω (deg) of the coin initial state given by Eq. (25) in the generalized elephant quantum walk with (a) $q = \infty$, (b) $q = 1/2$, and (c) $q = 1$. The values of θ and Ω considered to generate this graph were taken in intervals of 5° , from 0° to 90° . The average entanglement entropy for every point was obtained considering only the quasistationary part of the entropy time evolution and an initially localized walker was considered in all simulations.

obtained in Ref. [43], indicate that the generalized elephant quantum walk has the potential to generate maximally entangled coin states for almost all initial coin parameters and Kempe coin operators, considering $q \neq 1/2$ and an initially localized walker state.

In Fig. 4, we analyze the time-averaged entanglement entropy of the coin system as a function of the q parameter for some values of θ in the Kempe coin operator. From it, we observe that the entanglement entropy increases very fast in the interval $[0.5, 0.6]$ and goes asymptotically to $\langle S_E \rangle_t = 1$ as $q \rightarrow \infty$. Going back to the q -exponential function, changing from $q = 0.5$ to $q = 0.6$, we only increase the probability of having steps of size equal to 2 from 0 to approximately 6%. However, we have a substantial increase in the average entanglement, going from 0.8724 to 0.9852 for $\theta = \pi/4$, and

a moderate increase for $\theta = \pi/6$, from 0.9183 to 0.9878. With $\theta = \pi/18$, as the average entanglement with $q = 0.5$ is already significant [as can be seen in Fig. 3(b)], the increase is also small. In the long-time limit, changing the parameter q to one, the probability of unit step sizes is approximately 63%, of step sizes equal to two, approximately 23%, while of steps of sizes equal to three, 9%, but we already have an almost fully entangled state of $\langle S_E \rangle_t \approx 0.99$ for all θ . Consequently, considering an initially localized walker and the Kempe coin, we say that by allowing steps $\Delta_t = 2$ with a small probability, we enhance the generation of entanglement between the coin and position subsystems, with a strong randomness in the step sizes not being necessary, and the time-averaged coin von Neumann entropy almost reaches its maximum value with a probability of approximately 9% of $\Delta_t = 3$.

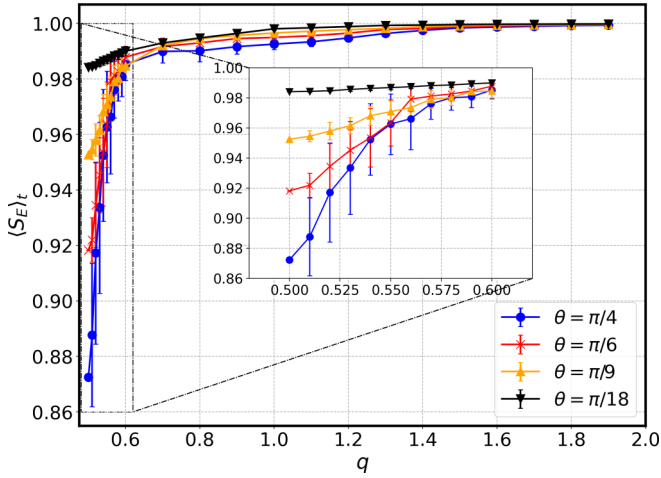


FIG. 4. Time-averaged entanglement entropy as a function of q in the q -exponential distribution given by Eq. (13) in the gEQW for different values of θ in the Kempe coin given by Eq. (5). The data points were obtained through the average of 50 simulations each and the error bars indicate the standard deviation of the points. In all simulations, the initial state was $|0\rangle \otimes (|\uparrow\rangle + |\downarrow\rangle)/\sqrt{2}$, i.e., $\Omega = \pi/2$ and $\phi = 0$.

We have studied how the time-averaged entanglement entropy of the gEQW for $\theta = \pi/4$ in Eq. (5) behaves as we change the coin initial state Bloch polar angle Ω . In Fig. 5, by varying Ω , we are able to control the increase of the entanglement entropy for q in the interval $[0.5, 0.6]$, where for $\Omega = 0$ the greatest rate is found. For $q > 0.6$, the entanglement entropy decreases, thus swapping the proportionality relation between Ω and the entanglement entropy by increasing parameter q , which only converges with the other curves at approximately $q = 1.6$.

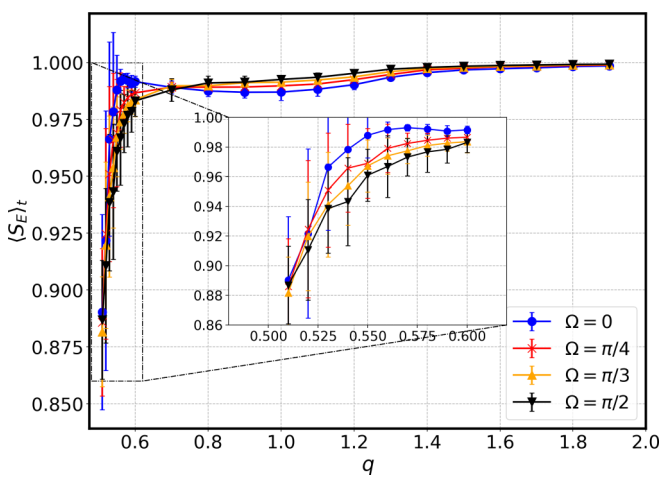


FIG. 5. Time-averaged entanglement entropy as a function of q in the q -exponential distribution given by Eq. (13) in the gEQW with the Kempe coin operator given by Eq. (5) with $\theta = \pi/4$ for different values of Ω using $\phi = 0$ for all of them. The data points were obtained through the average of 50 simulations each and the error bars indicate the standard deviation of the points. In all simulations, the localized initial state was used.

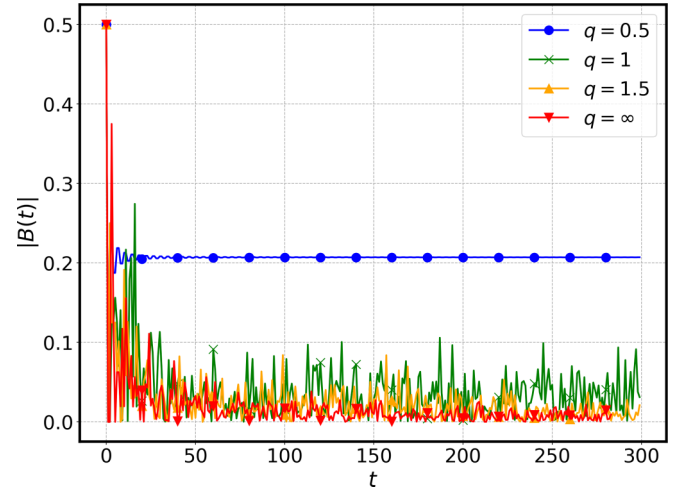


FIG. 6. Time evolution of the coin density matrix coherence absolute value for different generalized elephant quantum walks using $C_k(\pi/4)$. The initial state used in all simulations was the one localized on the origin and with the parameters $\phi = 0$ and $\Omega = \pi/2$ for the coin.

One can get a physical intuition as to why the generalized elephant quantum walk yields highly entangled states by remembering its open quantum walk interpretation. The surrounding environment that selects which unitary evolution the walker will go under introduces a decoherence effect in the coin evolution that can be revealed by the coin density coherence time evolution. Figure 6 shows the time evolution of the absolute value of $B(t)$ in the coin density matrix given by Eq. (20) for different q values of the generalized elephant quantum walk using the balanced Kempe coin. When considering the standard DTQW, $q = 0.5$, we see that the coherence absolute value has a decaying oscillating behavior, stabilizing into a value of approximately 0.2. By increasing the randomness on the step sizes, it decays even faster and stabilizes into lower values according to the degree of randomness, going to zero for the maximally random case, i.e., the EQW. This behavior is in agreement with the observed behavior of the average entanglement entropy as a function of q ; see Figs. 4 and 5.

Next, we investigate the time-averaged entanglement entropy by modifying the phase angles of the coin operator, given by Eq. (3), namely β , as depicted in the 3D plots of the mean entanglement entropy as a function of θ and β for $q = 0.5$ [Fig. 7(a)] and $q \rightarrow \infty$ [Fig. 7(b)].

Taking an initially localized walker state and $\Omega = \pi/2$ with $\phi = 0$, we understand that by varying the phase angle β in the standard quantum walk, the time-averaged entanglement entropy of the coin state does not change for a given value of θ , as $\langle S_E \rangle_t$ vs β remains constant. The same conclusion is drawn for the elephant quantum walk in Fig. 7(b). In addition, it does not matter whether we vary θ for a given value of β because $\langle S_E \rangle_t$ vs θ remains virtually constant. That is a strong indication that the generalized elephant quantum walk, for $q \neq 1/2$, produces highly entangled coin states, $S_E > 0.87$ for $q \in (0.5, 0.6]$, and maximally entangled coin

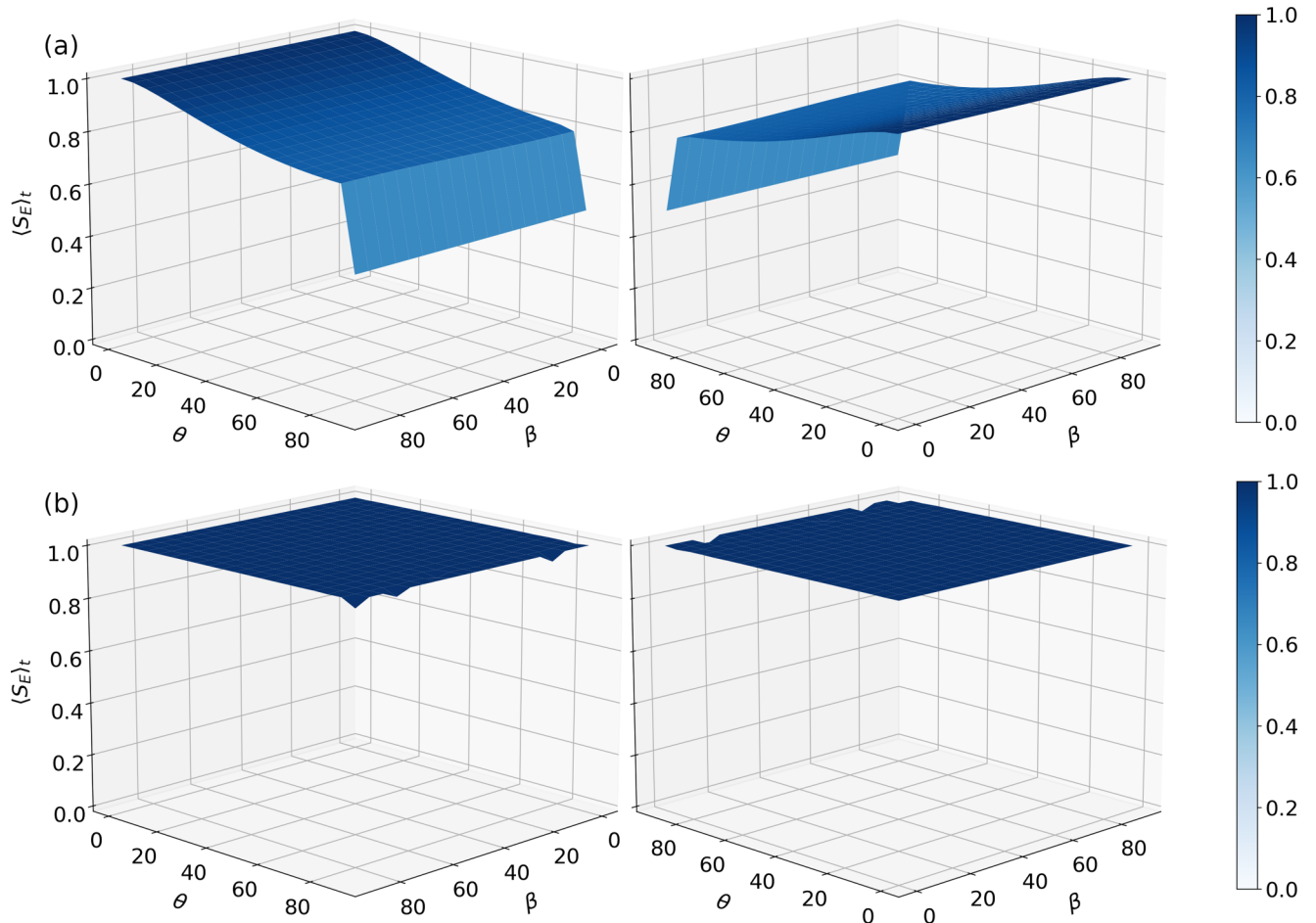


FIG. 7. Time-averaged entanglement entropy of the coin state in the generalized elephant quantum walk as a function of θ (deg) and β (deg) in the coin operator, given by Eq. (3). (a) $q = 0.5$; (b) $q = \infty$. All simulations were done considering an initially localized walker state and $\Omega = \pi/2$ and $\phi = 0$ in Eq. (25).

states for $q \rightarrow \infty$, for all coin operators and coin initial states, considering an initially localized walker state.

Following the above results, we survey the time-averaged coin von Neumann entropy for delocalized Gaussian walker initial states.

B. Delocalized initial states

The form of the delocalized position initial states that we considered is Gaussian,

$$|\psi_p(0)\rangle = \sum_{x=-\infty}^{\infty} N e^{-\frac{x^2}{4\sigma^2}} |x\rangle, \quad (26)$$

where N is a normalization factor and σ is the standard deviation of the distribution. In the standard DTQW, by using delocalized initial states, the position variance only gets a polynomial form in the short-time period, such as $\text{Var}_x(t) = a_0 + a_1 t + a_2 t^2$. Regarding the coin entanglement entropy, in Ref. [46] the asymptotic coin state was studied when one considers a Gaussian distribution for the position initial state as well, but for a Hadamard walk, given by Eq. (4). They found a relation between the coin initial state angles on the

Bloch sphere that gives a maximally entangled coin state,

$$\cos \phi = -\cot \Omega, \quad (27)$$

when the initial position variance $\sigma \gg 1$.

Aiming to capture the effect on the entanglement entropy of introducing randomness in the step sizes, we have computed the time evolution of the entanglement entropy for an initial coin state with $\Omega = \pi/3$ and $\phi \approx 0.696\pi$, following Eq. (27) in Fig. 8. In Fig. 8(a), we see that the quantum walk with random step sizes leads the entanglement entropy to the maximum value, while the same does not happen for the standard DTQW where an initially localized state is considered. That is in agreement with our previous results. However, as we change the variance of the initial position [Fig. 8(b)], the coin entanglement entropy gets to the maximal, reproducing previous results [46]. The only significant difference between the initially localized and delocalized states in the cases where we use the gEQW [Figs. 8(c) and 8(d)] is in the increase rate of the entanglement entropy as a function of time, where, as we increase σ , we get a slower $S_E(t)$ initial increase.

The following 3D plot shows the time-averaged entanglement entropy as a function of the Kempe coin operator parameter and the coin initial Bloch polar angle in the

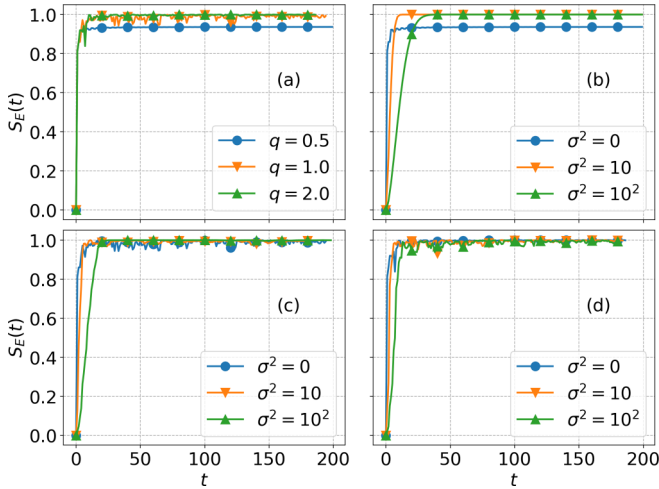


FIG. 8. Time evolution of the coin entanglement entropy for (a) different values of q and $\sigma^2 = 0$, and different values of σ for (b) $q = 0.5$, (c) $q = 1$, (d) $q = 2$ in the Hadamard walk. The coin initial state that was used is the one following Eq. (27) with $\Omega = \pi/3$.

standard DTQW [Fig. 9(a)], where we have considered a Gaussian initial state with $\sigma^2 = 10^3$. It can be seen that the

average coin entanglement entropy has lowered for all $\{\theta, \Omega\}$ pairs, with the maximum value obtained when we set $\theta = 0^\circ$ and $\Omega = 90^\circ$. For almost all pairs with $\theta > 20^\circ$, the coin entanglement entropy reaches its minimal value. In other words, the coin-position system is a separable one, something that happens only for a few points in the localized initial state case (see Fig. 3). Therefore, in the standard DTQW, the introduction of highly delocalized walker initial states drastically affects the asymptotic entanglement.

Figure 9(b) shows us the 3D plot of the elephant quantum walk case. Therein, we note that for almost all pairs, the average entanglement entropy is still close to its supreme, but with more oscillations around it. Furthermore, the behavior of the surface on the regions where $\theta \approx 0^\circ$ or $\theta \approx 90^\circ$ has significantly changed, with a decrease of $\langle S_E \rangle_t$ to 0.8 as θ goes to 90° and Ω goes to 0° . This scenario indicates that the coin entanglement entropy in the elephant quantum walk using the Kempe coin operator is robust against the use of highly delocalized walker initial states for a significant part of the set of possible $\{\theta, \Omega\}$ pairs, while this does not happen in the standard quantum walk.

Next, we investigate how the mean entanglement entropy varies as we change q in the q -exponential distribution with delocalized initial states. Figure 10 depicts the time-averaged

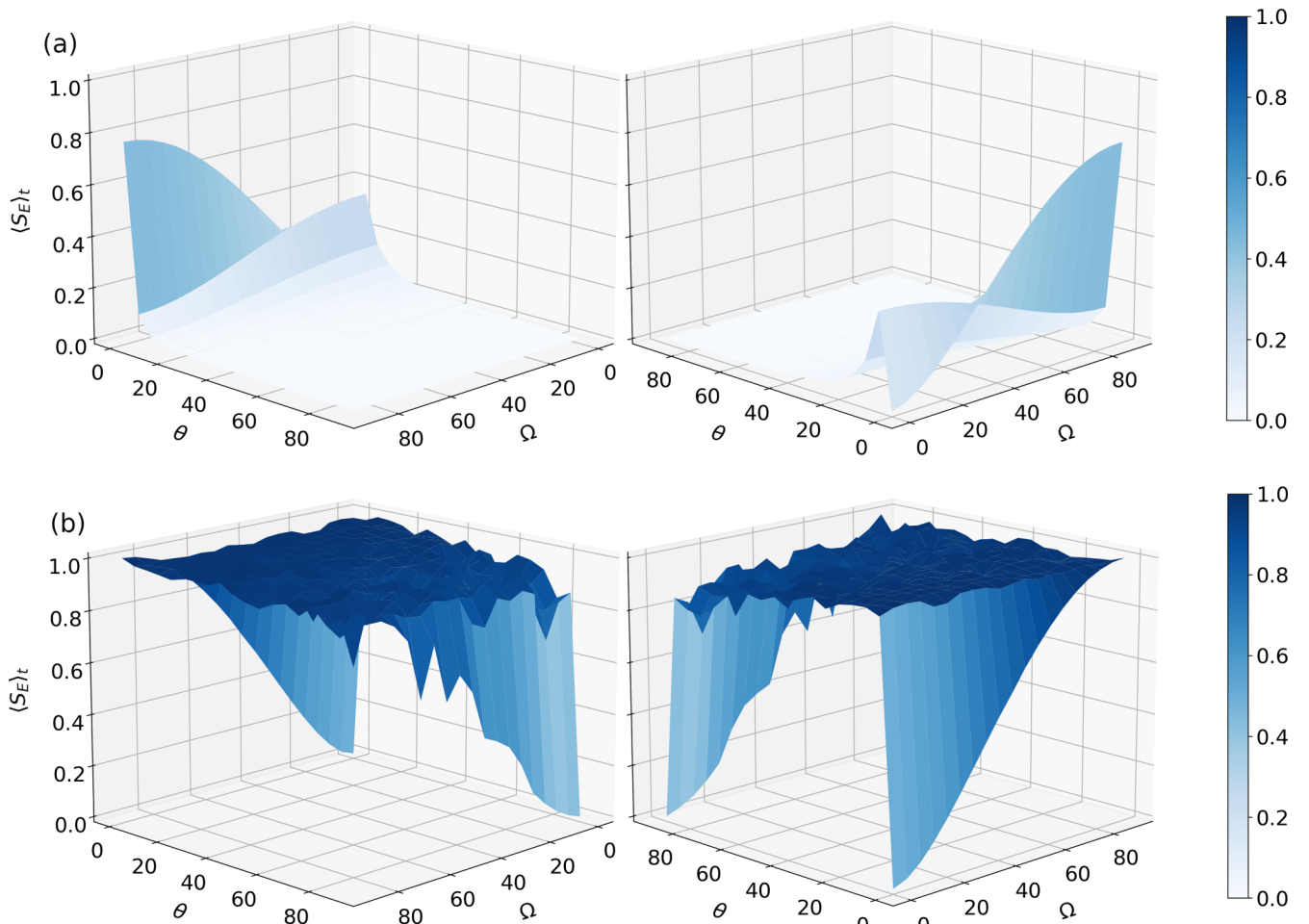


FIG. 9. Time-averaged entanglement entropy as a function of θ (deg) in Eq. (5) and Ω (deg) in Eq. (25) for the gEQW with (a) $q = 1/2$ and (b) $q = \infty$. The position initial state that was used is a Gaussian distribution given by Eq. (26) with $\sigma^2 = 10^3$ for both plots.

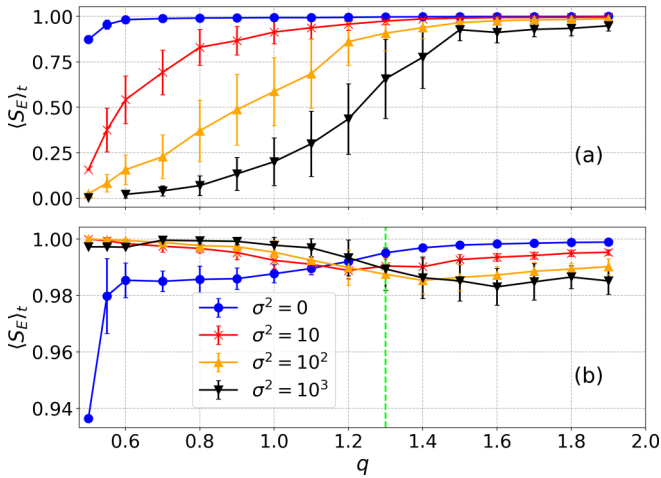


FIG. 10. Time-averaged coin entanglement entropy as a function of the q parameter in the gEQW with initially localized and delocalized position states. The coin operator used in (a) was Eq. (5) with $\theta = \pi/4$ and with $\Omega = \pi/2$ and $\phi = 0$, and in (b) the Hadamard operator with $\Omega = \pi/3$ and $\phi \approx 0.696\pi$. Each data point was obtained through 50 simulations.

entanglement entropy in the generalized elephant quantum walk as a function of q for different position initial variances in (a) with $\Omega = \pi/2$ and $\phi = 0$ and (b) with $\Omega = \pi/3$ and ϕ given by Eq. (27), in the coin initial state. Taking $q = 0.5$, we can see that the time-averaged entanglement indeed decreases as we increase the initial position variance, at least in the case where we use the Kempe coin operator with $\theta = \pi/4$ and $\Omega = \pi/2$ Fig. 10(a). We note that for $q \in (0.5, 1.5]$, the entanglement entropy decreases in comparison with the initially localized case as well; however, there is concomitantly an increase in the uncertainty of the data points. That can be assigned to the fact that the time evolution of the entanglement in the gEQW with q in this region presents very large oscillations, which in our interpretation indicates that with the use of initially delocalized states, the walker takes more time to reach the quasistationary regime. Nonetheless, comparing with the deterministic DTQW, we have an increase on the coin entropy and by inferring the asymptotic behavior of $\langle S_E \rangle_t$ vs q , we can say that this diminishing goes to zero as $q \rightarrow \infty$.

Considering Fig. 10(b), we see that the average entropy decreases, but in a smaller degree, as we increase q from 0.5 in the delocalized cases, being surpassed by the localized ones when $q = 1.3$. As in Fig. 10(a), that can be attributed to a delay in reaching the quasistationary regime by the use of delocalized initial states. Bridging those observations with the results obtained in Fig. 9(b), it is possible to assert that this decrease goes to zero as $q \rightarrow \infty$.

Finally, we look at the time-averaged coin entanglement entropy as a function of q for different values of θ in Eq. (5) and considering a Gaussian position initial state with (a) $\sigma^2 = 10$, (b) $\sigma^2 = 10^2$, and (c) $\sigma^2 = 10^3$ in Fig. 11. One sees that by varying θ , the mean entanglement curve changes significantly only as the initial position variance is low, indicating that with regard to the Kempe coin operator, the initial position variance plays a major role in the time-averaged coin entanglement entropy for greater values of σ .

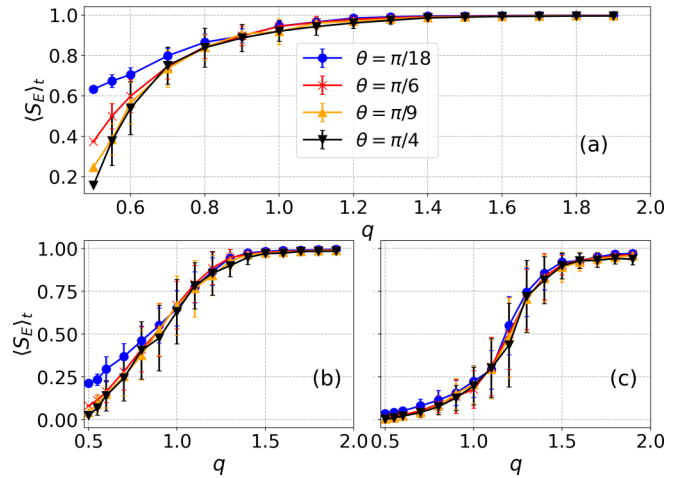


FIG. 11. Time-averaged entanglement entropy as a function of q considering different values of θ in the Kempe coin $C_k(\theta)$ given by Eq. (5) considering the initially delocalized gEQW, with (a) $\sigma^2 = 10$, (b) $\sigma^2 = 10^2$, and (c) $\sigma^2 = 10^3$, using the Kempe coin operator. In all simulations, a coin initial state was used with $\Omega = \pi/2$ and $\phi = 0$ in Eq. (25). Each data point was obtained through 50 simulations.

Let us briefly mention that for some important algorithmic applications, it is desired to control propagation as well as the way in which each spinor participates in the wave packet [63,64]. In this sense, we mention that the gEQW is also interesting as can be seen, for instance, in Fig. 12 where we quantify how much contribution each state provides to the full wave packet by means of the inverse participation ratio (IPR) of the probability distribution, $\text{IPR} \equiv \{\sum_x [P_t(x)]^2\}^{-1}$ [35,36,45,65–67]. Such measure has two extremes: (i) fully localized states where $P_t(x) = \delta_{x,0}$ and thus $\text{IPR} = 1$; (ii) fully delocalized states where $P_t(x) = 1/N$ and hence $\text{IPR} = N$, where N is the maximum possible number of sites in which

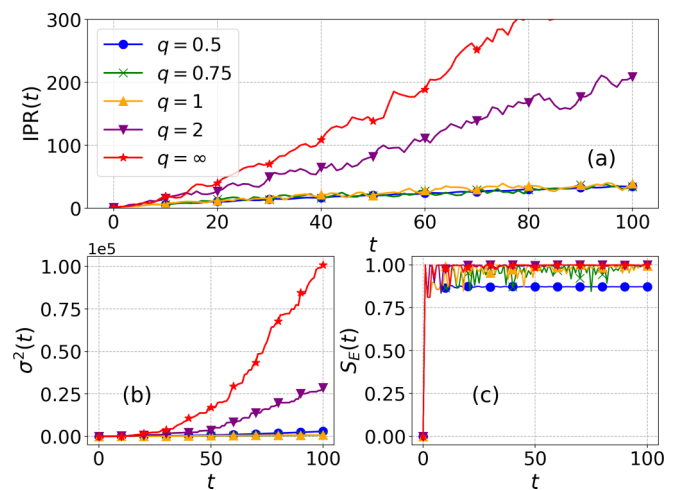


FIG. 12. IPR time series for (a) different generalized elephant quantum walks, (b) variance, and (c) von Neumann entropy time evolution for the same gEQWs. The coin operator used was $C_k(\pi/4)$ given by Eq. (5) and the initial state considered in all curves was the one localized in the origin with $\phi = 0$ and $\Omega = \pi/2$ in Eq. (25) as the coin initial state.

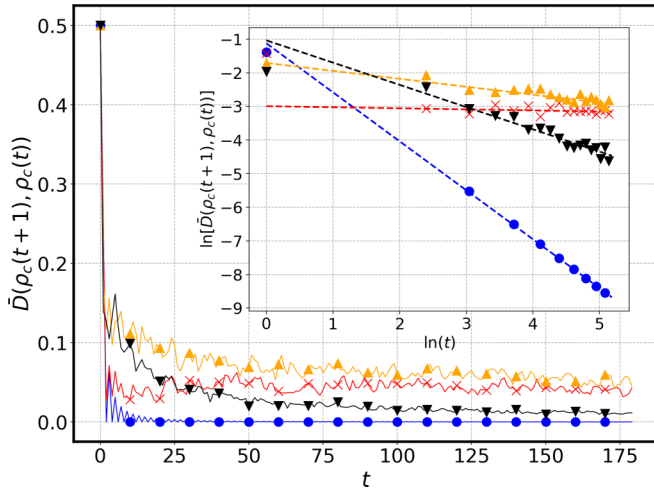


FIG. 13. Time evolution of the trace distance between two successive coin states for the initially localized gEQW with $q = 0.5$ (blue circle), $q = 0.6$ (red cross), $q = 1$ (orange up-triangle), and $q = \infty$ (black down-triangle). The coin initial state used was the one following Eq. (25) with $\Omega = \pi/2$ and $\phi = 0$, using $C_k(\pi/4)$ as the coin operator through the evolution. The size of the simulations sample considered for all curves, except $q = 0.5$, was 50. The inset shows the log-log graph of the same curves, with corresponding decay exponents $-\beta$, (-1.456 ± 0.004) for $q = 0.5$, (-0.03 ± 0.02) for $q = 0.6$, (-0.236 ± 0.008) for $q = 1$, and (-0.66 ± 0.01) for $q = \infty$.

$P_i(x)$ can be distributed. We see in Fig. 12 that by tuning q , it is possible to engineer changes in the probability distribution $P_i(x)$ in a way that we can control propagation as well as spatial participation of each spinor in the full wave packet without reducing the coin-position entanglement.

C. Quasistationary regime

To analyze the long-time behavior of the quantum coin evolution with regard to its state changes, we have to use a measure of distinctness between quantum states. For that reason, we have employed the trace distance,

$$D(\rho, \sigma) = \frac{1}{2} \|\rho - \sigma\|_1, \quad (28)$$

where $\|A\|_1 = \text{tr}\sqrt{AA^\dagger}$ is the matrix 1-norm. If $\rho = \sigma$, then the trace distance between them is zero and if they are matrices representing orthogonal states, i.e., $\sigma = \rho^\perp$, their distance is maximum. Hence, by calculating the trace distance between two successive states, $D[\rho_c(t+1), \rho_c(t)]$, we can find how, if so, the generalized elephant quantum walk goes to the quasistationary regime, which here we define as the dynamics time regime in which the trace distance between two successive states is constant on average, being zero in the limit of a true stationary regime.

We begin by looking at the trace distance evolution for different generalized elephant quantum walks, with the standard DTQW included, using initially localized walker states. For $q \neq 0.5$, given that the evolution is stochastic, the trace distance considered is an ensemble average. From Fig. 13, we

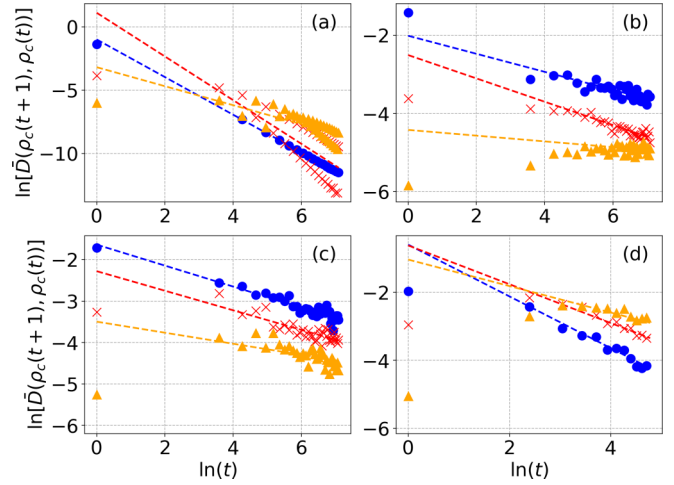


FIG. 14. Log-log graphs of the average trace distance between two successive coin states' time evolution in the generalized elephant quantum walk using $C_k(\pi/4)$ as the coin operator with $\phi = 0$ and $\Omega = \pi/2$ determining the coin initial state with different initial variances. The initial variances are $\sigma^2 = 0$ (blue circle), $\sigma^2 = 10$ (red star), and $\sigma^2 = 10^2$ (orange up-triangle). In (a), we have the standard DTQW, (b) $q = 0.6$, (c) with $q = 1.0$, and (d) corresponding to $q = \infty$. The average was calculated through 50 simulations for each curve.

can see that the trace distance decays following a power law in time, $\bar{D} \propto t^{-\beta}$. Also, by increasing the amount of randomness, the quantum walk goes to the stationary regime slower than in the deterministic case, with the decay law exponent β —given by the log-log inset fittings—equal to approximately 1.5 for the standard DTQW, $\beta \approx 0.03$ for $q = 0.6$, $\beta \approx 0.24$ for $q = 1$, and $\beta \approx 0.66$ for the elephant quantum walk. Moreover, it is possible to affirm that the decay exponent does not follow a simple inverse relationship with the amount of randomness since the decay exponent for the completely random case is greater than for $q = 0.6$ and $q = 1$.

Now we move to see what are the effects of using an initially delocalized state. As a means of comparison, first we look at the standard DTQW trace distance [Fig. 14(a)]. It is possible to note that the use of initially delocalized states introduces oscillations and a transient regime in evolution that is made longer when we increase the initial variance. Moreover, by fitting the data points for $t \gg 1$ into a power law and calculating the decay exponents (Table I), we see that by increasing the initial delocalization, the quantum walk reaches

TABLE I. Table of the decay exponent β of the trace distance between two time successive states considering the different values of q and initial variance σ^2 obtained through the fittings of the curves for $t \gg 1$ in Fig. 14.

$q \backslash \sigma^2$	0	10	10^2
0.5	1.487 ± 0.001	1.73 ± 0.04	0.75 ± 0.02
0.6	0.23 ± 0.01	0.30 ± 0.01	0.07 ± 0.01
1	0.253 ± 0.003	0.236 ± 0.005	0.133 ± 0.006
∞	0.76 ± 0.02	0.57 ± 0.02	0.37 ± 0.03

the quasistationary regime faster than in the localized case when $\sigma^2 = 10$ (red cross curve) but slower when $\sigma^2 = 10^2$ (orange up-triangle curve). Besides the fact that a true stationary regime does not exist, for the quantum walks with random step sizes, $q = 0.6$ [Fig. 14(b)], $q = 1$ [Fig. 14(c)], and $q = \infty$ [Fig. 14(d)], the same features are observed. With $q = 0.6$, when we use $\sigma^2 = 10$, the quasistationary regime is achieved faster than in the localized case, but with $\sigma^2 = 10^2$, it is achieved much more slowly, with a longer initial transient increasing. As we increase the amount of randomness, this transient takes much more time, as we can note from Figs. 14(c) and 14(d), and we do not observe a faster decay for $\sigma^2 = 10$ (see Table I).

This property of retarding the quasistationary regime as one increases the initial delocalization explains the greater uncertainty and lower values of the average entanglement of Fig. 10 when one also increases the amount of randomness. It is also remarkable that the feature of extending the transient regime was previously observed in quantum walks with dynamically random coin operators [27], where the decaying trace distance follows a power law with exponent equal to $-1/4$. This tells us that this property is indeed a feature of dynamically random quantum walks, now including the use of random shift operators. We highlight that Figs. 13 and 14 can also be used as evidence that on average, the quantum walks with random steps sizes indeed have a quasistationary regime, with some of them taking more time than others to reach it, depending on the initial delocalization and degree of randomness of the step sizes.

V. FINAL REMARKS

We have analyzed the production of coin entanglement entropy in the generalized elephant quantum walk considering different types of initial conditions and coin operators.

First, looking at the initially localized walker state, we have observed that the time-averaged coin entanglement reaches its maximum value for almost all parameters in the Kempe coin operator and polar angles in the coin initial state Bloch sphere when the step distribution is uniform and exponential [Figs. 3(a) and 3(c)], i.e., with $q = \infty$ and $q = 1$ in the distribution parameter, respectively. That behavior does not occur in the standard discrete-time quantum walk considering the same parameters, as presented in Fig. 3(b). On the other hand, when we have used a more general type of coin operator for the same initial walker state, given by Eq. (3), we learned the elephant quantum walk entanglement does not change [Fig. 7(b)], while in the DTQW [Fig. 7(a)], the time-averaged entanglement entropy can vary from its value given when we use $\theta = \pi/4$ in the Kempe coin up to almost the maximum value. Looking at the $\langle S_E \rangle_t$ vs q (Figs. 4 and 5), we have seen that it only takes a small amount of disorder in order to greatly improve the time-averaged entanglement, going from $\langle S_E \rangle_t \approx 0.8724$ with only unit step sizes to 0.9852 with probability of approximately 6% of having steps of sizes equal to 2 ($q = 0.6$), for $\theta = \pi/4$. By changing the Kempe coin parameter, one only increases the initial entanglement average as a function of q increase rate, and

the same goes for the Bloch polar angle of the coin initial state.

Next, we have considered the use of Gaussian delocalized initial states, and the use of random steps sizes also improved the time-averaged coin entanglement when one uses the Kempe coin operator and $\Omega = \pi/2$ and $\phi = 0$ in the coin initial state. However, by analyzing the dependence of the average entanglement on the amount of disorder, we have learned that for $q \in (0.5, 1.5]$, the uncertainty of the data increased, indicating a possible retarding on reaching the quasistationary regime. This has been confirmed by an analysis of the quasistationary regime through the trace distance between two time successive coin states. By comparing the initially localized and delocalized walks, we found that when one increases the initial randomness, the initial transient regime becomes longer. Looking at the stationary regime, the power-law exponent describing the trace distance decay, in both localized and delocalized walks, becomes greater than the deterministic case, something that was also observed in quantum walks with dynamically random coin operators. Nonetheless, we assert that for almost all initial coin states and coin operators, the generalized elephant quantum walk enhances the coin entanglement entropy for delocalized initial states, taking it to the supreme as $q \rightarrow \infty$.

Although it is usually expected that disorder weakens quantum features, nowadays it has already been established by numerical [26], theoretical [27], and experimental [23,24] work that dynamical disorder embedded in the coin operator of QWs acts as a maximal entanglement generator. Such strengthening of the entanglement takes place at the cost of weakening the controllability of the spreading features. In sharp contrast, novel properties emerge when the dynamical disorder is embedded in the shift operator of QWs [52]. The generalized elephant quantum walk (gEQW) [43] is a protocol that has a remarkable variety of scaling behavior (diffusive, superdiffusive, ballistic, hyperballistic, as shown in Fig. 2) and still produces maximally entangled coin states. Such features make the gEQW an interesting protocol for potential applications demanding controllability of transport properties while keeping a maximum asymptotic entanglement. However, in order to move on towards future applications, it is necessary to understand whether the enhancement of the entanglement of the gEQW is robust or only valid for the specific coin operators and local states studied in Ref. [43]. Here, we have shown that such highly entangled states are also achieved with delocalized initial states and general coin operators in a robust way.

That being said, we conclude that disordered quantum walks—either with dynamical disorder in the coin operator or in the shift operator—generate maximally entangled coin states for almost all initial coin states and coin operators considering initially localized walkers, and, for the delocalized ones in the limit $q \rightarrow \infty$, the same is guaranteed.

In summary, we have extensively shown that the application of dynamically disordered QWs as a maximal entanglement generator is also possible when (i) the temporal disorder is embedded in the step operator and (ii) general coin operators and both local and delocalized initial states are used.

We highlight that differently from all previous QW-based protocols for generating highly entangled states—that do not allow high controllability of the spreading—our protocol opens the doors for potential new possibilities of applications of dynamically disordered QWs as a robust maximal entanglement generator in programmable setups that range from slower than ballistic to faster than ballistic.

In quantum simulations, the primary objective is to engineer a quantum system that could be tuned to model the properties of other quantum systems. In this sense, it is evident from our work that the rich spreading phenomenology of the gEQW accompanied by a robust amplification entanglement captures the essence of a programmable quantum system.

In future works, we aim to investigate to what extent it is possible to optimize the efficiency of our setup for gen-

erating highly entangled states without losing the richness of the spreading behavior (diffusive, superdiffusive, ballistic, hyperballistic).

ACKNOWLEDGMENTS

C.B.N. acknowledges the support from IFSC-USP and from Coordenação de Aperfeiçoamento de Pessoal de Nível Superior - Brasil (CAPES) - Finance Code 001. M.A.P. acknowledges the support by the funding agency FUNCAP. D.O.S.P. acknowledges the support by the Brazilian funding agencies CNPq (Grant No. 307028/2019-4), FAPESP (Grant No. 2017/03727-0), and the Brazilian National Institute of Science and Technology of Quantum Information (INCT/IQ). S.M.D.Q. acknowledges the financial support from CNPq Grant No. 307028/2019-4.

-
- [1] Y. Aharonov, L. Davidovich, and N. Zagury, Quantum random walks, *Phys. Rev. A* **48**, 1687 (1993).
- [2] Frontiers, Feynman's "quantum walk" observed, *Phys. World* **22**, 4 (2009).
- [3] A. Widera, A walk across a quantum lattice, *Science* **347**, 1200 (2015).
- [4] M. Mohseni, P. Rebentrost, S. Lloyd, and A. Aspuru-Guzik, Environment-assisted quantum walks in photosynthetic energy transfer, *J. Chem. Phys.* **129**, 174106 (2008).
- [5] S. E. Venegas-Andraca, Quantum walks for computer scientists, *Synth. Lect. Quantum Comput.* **1**, 1 (2008).
- [6] R. Portugal, *Quantum Walks and Search Algorithms* (Springer, New York, 2013).
- [7] A. Ambainis, Quantum walks and their algorithmic applications, *Intl. J. Quantum Inf.* **01**, 507 (2003).
- [8] J. Kempe, Quantum random walks: An introductory overview, *Contemp. Phys.* **44**, 307 (2003).
- [9] V. M. Kendon, A random walk approach to quantum algorithms, *Philos. Trans. R. Soc. A* **364**, 3407 (2006).
- [10] K. Kadian, S. Garhwal, and A. Kumar, Quantum walk and its application domains: A systematic review, *Comput. Sci. Rev.* **41**, 100419 (2021).
- [11] T. Kitagawa, Topological phenomena in quantum walks: Elementary introduction to the physics of topological phases, *Quantum Inf. Proc.* **11**, 1107 (2012).
- [12] J. Wu, W.-W. Zhang, and B. C. Sanders, Topological quantum walks: Theory and experiments, *Front. Phys.* **14**, 61301 (2019).
- [13] M. Gräfe, R. Heilmann, M. Lebugle, D. Guzman-Silva, A. Perez-Leija, and A. Szameit, Integrated photonic quantum walks, *J. Opt.* **18**, 103002 (2016).
- [14] M. Gräfe and A. Szameit, Integrated photonic quantum walks, *J. Phys. B: At., Mol. Opt. Phys.* **53**, 073001 (2020).
- [15] J. Wang and K. Manouchehri, *Physical Implementation of Quantum Walks* (Springer, New York, 2013).
- [16] L. Neves and G. Puentes, Photonic discrete-time quantum walks and applications, *Entropy* **20**, 731 (2018).
- [17] N. Stamatopoulos, D. J. Egger, Y. Sun, C. Zoufal, R. Iten, N. Shen, and S. Woerner, Option pricing using quantum computers, *Quantum* **4**, 291 (2020).
- [18] L. K. Grover, A fast quantum mechanical algorithm for database search, in *Proceedings of the Twenty-Eighth Annual ACM Symposium on Theory of Computing*, STOC '96 (Association for Computing Machinery, New York, 1996), pp. 212–219.
- [19] I. Carneiro, M. Loo, X. Xu, M. Girerd, V. Kendon, and P. L. Knight, Entanglement in coined quantum walks on regular graphs, *New J. Phys.* **7**, 156 (2005).
- [20] *Anderson Localization and its Ramifications: Disorder, Phase Coherence and Electron Correlations*, edited by T. Brandes and S. Kettemann (Springer, New York, 2003).
- [21] S. Stützer, T. Kottos, A. Tünnermann, S. Nolte, D. Christodoulides, and A. Szameit, Superballistic growth of the variance of optical wave packets, *Opt. Lett.* **38**, 4675 (2013).
- [22] G. Abal, R. Siri, A. Romanelli, and R. Donangelo, Quantum walk on the line: Entanglement and nonlocal initial conditions, *Phys. Rev. A* **73**, 042302 (2006).
- [23] Q.-Q. Wang, X.-Y. Xu, W.-W. Pan, K. Sun, J.-S. Xu, G. Chen, Y.-J. Han, C.-F. Li, and G.-C. Guo, Dynamic-disorder-induced enhancement of entanglement in photonic quantum walks, *Optica* **5**, 1136 (2018).
- [24] S.-J. Tao, Q.-Q. Wang, Z. Chen, W.-W. Pan, S. Yu, G. Chen, X.-Y. Xu, Y.-J. Han, C.-F. Li, and G.-C. Guo, Experimental optimal generation of hybrid entangled states in photonic quantum walks, *Opt. Lett.* **46**, 1868 (2021).
- [25] Q.-P. Su, Y. Zhang, L. Yu, J.-Q. Zhou, J.-S. Jin, X.-Q. Xu, S.-J. Xiong, Q. Xu, Z. Sun, K. Chen *et al.*, Experimental demonstration of quantum walks with initial superposition states, *npj Quantum Inf.* **5**, 40 (2019).
- [26] C. Chandrashekar, Disorder induced localization and enhancement of entanglement in one- and two-dimensional quantum walks, *arXiv:1212.5984*.
- [27] R. Vieira, E. P. M. Amorim, and G. Rigolin, Dynamically Disordered Quantum Walk as a Maximal Entanglement Generator, *Phys. Rev. Lett.* **111**, 180503 (2013).
- [28] S. Salimi and R. Yosefjani, Asymptotic entanglement in 1d quantum walks with a time-dependent coined, *Intl. J. Mod. Phys. B* **26**, 1250112 (2012).
- [29] P. P. Rohde, G. K. Brennen, and A. Gilchrist, Quantum walks with memory provided by recycled coins and a memory of the coin-flip history, *Phys. Rev. A* **87**, 052302 (2013).
- [30] R. Vieira, E. P. M. Amorim, and G. Rigolin, Entangling power of disordered quantum walks, *Phys. Rev. A* **89**, 042307 (2014).

- [31] G. Di Molfetta and F. Debbasch, Discrete-time quantum walks in random artificial gauge fields, *Quantum Stud.: Math. Found.* **3**, 293 (2016).
- [32] A. C. Orthey and E. P. Amorim, Weak disorder enhancing the production of entanglement in quantum walks, *Braz. J. Phys.* **49**, 595 (2019).
- [33] S. Singh, R. Balu, R. Laflamme, and C. Chandrashekar, Accelerated quantum walk, two-particle entanglement generation and localization, *J. Phys. Commun.* **3**, 055008 (2019).
- [34] M. Montero, Classical-like behavior in quantum walks with inhomogeneous, time-dependent coin operators, *Phys. Rev. A* **93**, 062316 (2016).
- [35] M. Zeng and E. H. Yong, Discrete-time quantum walk with phase disorder: Localization and entanglement entropy, *Sci. Rep.* **7**, 12024 (2017).
- [36] A. R. C. Buarque and W. S. Dias, Aperiodic space-inhomogeneous quantum walks: Localization properties, energy spectra, and enhancement of entanglement, *Phys. Rev. E* **100**, 032106 (2019).
- [37] M. A. Pires and Silvio M. Duarte Queirós, Parrondo's paradox in quantum walks with time-dependent coin operators, *Phys. Rev. E* **102**, 042124 (2020).
- [38] A. Gratsea, M. Lewenstein, and A. Dauphin, Generation of hybrid maximally entangled states in a one-dimensional quantum walk, *Quantum Sci. Technol.* **5**, 025002 (2020).
- [39] A. Gratsea, F. Metz, and T. Busch, Universal and optimal coin sequences for high entanglement generation in 1d discrete time quantum walks, *J. Phys. A: Math. Theor.* **53**, 445306 (2020).
- [40] Z. Walczak and J. H. Bauer, Parrondo's paradox in quantum walks with deterministic aperiodic sequence of coins, *Phys. Rev. E* **104**, 064209 (2021).
- [41] M. A. Pires and S. M. D. Queirós, Negative correlations can play a positive role in disordered quantum walks, *Sci. Rep.* **11**, 1 (2021).
- [42] R. Zhang, R. Yang, J. Guo, C.-W. Sun, J.-C. Duan, H. Zhou, Z. Xie, P. Xu, Y.-X. Gong, and S.-N. Zhu, Maximal coin-walker entanglement in a ballistic quantum walk, *Phys. Rev. A* **105**, 042216 (2022).
- [43] M. A. Pires, G. Di Molfetta, and S. M. D. Queirós, Multiple transitions between normal and hyperballistic diffusion in quantum walks with time-dependent jumps, *Sci. Rep.* **9**, 1 (2019).
- [44] P. Sen, Scaling and crossover behaviour in a truncated long range quantum walk, *Physica A* **545**, 123529 (2020).
- [45] M. A. Pires and S. M. Duarte Queirós, Quantum walks with sequential aperiodic jumps, *Phys. Rev. E* **102**, 012104 (2020).
- [46] A. C. Orthey and E. P. Amorim, Asymptotic entanglement in quantum walks from delocalized initial states, *Quantum Inf. Proc.* **16**, 224 (2017).
- [47] O. Mülken, V. Pernice, and A. Blumen, Universal behavior of quantum walks with long-range steps, *Phys. Rev. E* **77**, 021117 (2008).
- [48] M. O. Cáceres and M. Nizama, The quantum Levy walk, *J. Phys. A: Math. Theor.* **43**, 455306 (2010).
- [49] H. Lavička, V. Potoček, T. Kiss, E. Lutz, and I. Jex, Quantum walk with jumps, *Eur. Phys. J. D* **64**, 119 (2011).
- [50] J. Zhao and P. Tong, One-dimensional quantum walks subject to next-nearest-neighbour hopping decoherence, *Quantum Inf. Proc.* **14**, 2357 (2015).
- [51] T. Chattaraj and R. V. Krems, Effects of long-range hopping and interactions on quantum walks in ordered and disordered lattices, *Phys. Rev. A* **94**, 023601 (2016).
- [52] G. Di Molfetta, D. O. Soares-Pinto, and Silvio M. Duarte Queirós, Elephant quantum walk, *Phys. Rev. A* **97**, 062112 (2018).
- [53] S. Das, S. Mal, A. Sen(De), and U. Sen, Inhibition of spreading in quantum random walks due to quenched poisson-distributed disorder, *Phys. Rev. A* **99**, 042329 (2019).
- [54] P. Sen, Unusual scaling in a discrete quantum walk with random long range steps, *Physica A* **514**, 266 (2019).
- [55] S. Mukhopadhyay and P. Sen, Persistent quantum walks: Dynamic phases and diverging timescales, *Phys. Rev. Res.* **2**, 023002 (2020).
- [56] A. Zaman, R. Ahmad, S. Bibi, and S. Khan, Randomizing quantum walk, *Intl. J. Theor. Phys.* **61**, 135 (2022).
- [57] G. A. Domínguez-Castro and R. Paredes, Enhanced transport of two interacting quantum walkers in a one-dimensional quasicrystal with power-law hopping, *Phys. Rev. A* **104**, 033306 (2021).
- [58] S. E. Venegas-Andraca, Quantum walks: A comprehensive review, *Quantum Inf. Proc.* **11**, 1015 (2012).
- [59] D. Reitzner, Quantum walks, *Acta Physica Slovaca.* **61**, 603 (2011).
- [60] G. M. Schütz and S. Trimper, Elephants can always remember: Exact long-range memory effects in a non-Markovian random walk, *Phys. Rev. E* **70**, 045101(R) (2004).
- [61] C. Tsallis, Nonadditive entropy and nonextensive statistical mechanics—An overview after 20 years, *Braz. J. Phys.* **39**, 337 (2009).
- [62] R. Horodecki, P. Horodecki, M. Horodecki, and K. Horodecki, Quantum entanglement, *Rev. Mod. Phys.* **81**, 865 (2009).
- [63] V. Kendon and B. Tregenna, Decoherence can be useful in quantum walks, *Phys. Rev. A* **67**, 042315 (2003).
- [64] G. Martín-Vázquez and J. Rodríguez-Laguna, Optimizing the spatial spread of a quantum walk, *Phys. Rev. A* **102**, 022223 (2020).
- [65] J. Ghosh, Simulating Anderson localization via a quantum walk on a one-dimensional lattice of superconducting qubits, *Phys. Rev. A* **89**, 022309 (2014).
- [66] İ. Yalçinkaya and Z. Gedik, Two-dimensional quantum walk under artificial magnetic field, *Phys. Rev. A* **92**, 042324 (2015).
- [67] S. Derevyanko, Anderson localization of a one-dimensional quantum walker, *Sci. Rep.* **8**, 1795 (2018).